Manuscript type: Technique

A water-soluble, synthetic auxin analog for rapid degradation of target proteins during *C. elegans* development

Michael A. Martinez[a], Brian A. Kinney[b], Guinevere Ashley[c], James M. Ragle[c], Christopher M. Hammell[b], Jordan D. Ward[c], David Q. Matus[a,*]

[a]Department of Biochemistry and Cell Biology, Stony Brook University, Stony Brook, NY 11794, USA.

[b]Walter B. James Laboratory, Cold Spring Harbor Laboratory, Cold Spring Harbor, NY 11724, USA.

[c]Department of Molecular, Cell, and Developmental Biology, University of California-Santa Cruz, Santa Cruz, CA 95064, USA.

[*]Correspondence to David Q. Matus: david.matus@stonybrook.edu

HIGHLIGHTS

- Within 30 minutes AID-tagged proteins can be >80% depleted relative to wild-type levels using a water-soluble synthetic auxin analog
- The endogenous *C. elegans* SKP1-CUL1-F-box (SCF) complex mediates auxin-dependent degradation
- Temporal depletion of AID-tagged Ftz-F1/*nhr-25* affects both cell fate specification and cell division during *C. elegans* uterine-vulval development
- Synthetic auxin can be utilized in microfluidics-based assays to deplete target proteins

ABSTRACT

As developmental biologists in the age of genome editing, we now have access to an ever-increasing array of tools to manipulate endogenous gene expression. By combining CRISPR/Cas9-genome engineering with heterologous systems for targeted protein degradation, researchers can gain the spatial and temporal control to dissect endogenous protein function during development. A recent addition to this toolkit is the auxin-inducible degradation system, which functions through the activity of a hormone-inducible *Arabidopsis* F-box protein, transport inhibitor response 1 (TIR1). In the presence of auxin, TIR1 serves as a substrate recognition component of the E3 ubiquitin ligase complex SKP1-CUL1-F-box (SCF), ubiquitinating auxin-inducible degron (AID)-tagged proteins for proteasomal degradation. This system has been used successfully in *C. elegans*, *Drosophila*, zebrafish, yeast, and mammalian cell culture for rapid targeted protein depletion. Here, we describe an improved protocol for the AID system in *C. elegans*, utilizing a cost-effect alternative to the natural auxin indole-3-acetic acid (IAA), 1-naphthaleneacetic acid (NAA). We take advantage of the increased water solubility of NAA and demonstrate through quantitative high-resolution spinning disk confocal microscopy that we can rapidly degrade target proteins within 30 minutes of NAA exposure. Additionally, we find that NAA works robustly in both growth media and aqueous buffer, allowing for comparative use among growth plates, liquid submersion and microfluidic devices. We provide evidence that TIR1 interacts with *C. elegans* CUL1 homolog, *cul-1,* to degrade target proteins. Finally, as a proof-of-principle, we demonstrate high-throughput, penetrant defects from AID-mediated depletion of the Ftz-F1 nuclear hormone receptor, *nhr-25*, during *C. elegans* uterine-vulval development, where early depletion of *nhr-25* results in a failure to specify the uterine anchor cell and later depletion arrests the division of the vulval precursor cells that give rise to the adult egg-laying apparatus. Together, this work provides a streamlined protocol broadly applicable to targeted protein degradation methods for dissecting gene function throughout *C. elegans* development and homeostasis.

KEYWORDS

C. elegans; AID; NAA; CUL-1; NHR-25; Microfluidics

INTRODUCTION

In situ techniques for targeted protein degradation enable a detailed analysis of developmental events, mechanisms and functions. Targeting proteins for degradation in specific metazoan tissues overcomes a limitation set by genome-editing technologies (Hubbard, 2014; Qadota et al., 2007; Shen et al., 2014) where a persistence of the target protein following DNA or RNA manipulation can delay the manifestation of an otherwise acute phenotype. Several methods have been described recently to enable tissue-specific protein degradation in *C. elegans*, including ZF1 tagging (Armenti et al., 2014), a GFP nanobody approach (Wang et al., 2017), sortase A (Wu et al., 2017), and auxin-mediated degradation (Zhang et al., 2015).

The auxin-inducible degradation system, the focus of this report, allows rapid and conditional degradation of auxin-inducible degron (AID)-tagged proteins in *C. elegans* as well as in other commonly used model systems including yeast (Nishimura et al., 2009), *Drosophila* (Trost et al., 2016), zebrafish (Daniel et al., 2018), and cultured mammalian cells (Holland et al., 2012; Nishimura et al., 2009). This protein degradation system relies on the expression of an *Arabidopsis* F-box protein called transport inhibitor response 1 (TIR1). As a substrate-recognition component of the E3 ubiquitin ligase complex SKP1-CUL1-F-box (SCF), TIR1 carries out its function only in the presence of the hormone auxin, and once bound to auxin, targets AID-tagged proteins for ubiquitin-dependent proteasomal degradation (**Figure 1**).

The auxin-inducible degradation system in *C. elegans* is robust and specific with minimal off-target effects (Zhang et al., 2015). However, further exploration of the system is needed to assess its utility among *C. elegans* researchers conducting single-cell biology within a narrow developmental time frame. Here, we report a rapid, optimized method that utilizes 1-naphthaleneacetic acid (NAA), a synthetic analog of the natural auxin indole-3-acetic acid (IAA), that is water-soluble, stable, and inexpensive. Additionally, based on quantitative measurements at single-cell resolution, using NAA, we demonstrated comparable protein degradation kinetics as observed using IAA. Unlike current auxin treatment methods, this synthetic auxin analog can be solubilized in M9 buffer in a time-efficient, cost-effective, and non-toxic manner, and as a result, we also pair its use with *C. elegans*-based microfluidics for the first time. As a proof-of-principle, we modulated the activity of endogenous NHR-25, the single *C. elegans* homolog of *Drosophila* Ftz-F1, and mammalian SF-1 and LRH-1, which plays well-characterized roles in vulval development (Chen et al., 2004; Ward et al., 2013). Using live-cell imaging, we explored the ability of NAA to induce targeted degradation of the endogenous NHR-25 protein in the developing uterus and vulva. It is our hope that this synthetic auxin analog can be applied at all stages of *C. elegans* development allowing for precise, rapid degradation of target proteins in a high-throughput and quantitative fashion.

MATERIALS AND METHODS

Constructs and microinjection

SapTrap was used to construct the 30xlinker::GFP^SEC^TEV::AID degron::3xFLAG repair template (pJW1747) for generating the knock-in into the 3' end of the *nhr-25* gene (Schwartz and Jorgensen, 2016). DH10 β competent *E.coli* cells, made in house, were used for generating the plasmid. The following reagents were used to assemble the final repair template: pDD379 (backbone with F+E sgRNA), annealed oligos 3482+3483 (sgRNA), pJW1779 (5' homology arm), 3' homology arm PCR product, pJW1347 (30x linker for CT slot), pDD372 (GFP for FP slot), pDD363 (SEC with LoxP sites), and pJW1759 (TEV::AID degron::3xFLAG for NT slot).

The pJW1747 repair template was purified using the Invitrogen PureLink HQ Mini Plasmid DNA Purification Kit (K210001). The optional wash step in the protocol using a 4 M guanidine-HCl + 40% isopropanol solution is highly recommended as excluding it dramatically reduced injection efficiency in our hands. N2 animals were injected with a mix consisting of 10 ng/µl pJW1747, 50 ng/µl of pDD121 (Cas9 vector), and co-injection markers (10 ng/µl pGH8, 5 ng/µl pCFJ104, 2.5 ng/µl pCFJ90) as previously described (Dickinson et al., 2015, 2013; Frøkjær-Jensen et al., 2012). Knock-ins were isolated as previously described (Dickinson et al., 2015). Each knock-in junction was verified via PCR using a primer that bound outside the homology arm paired with a primer binding within pJW1747 (see **Key Resources Table**). The knock-in was backcrossed five times against wildtype N2 animals to produce JDW58. The SEC was then excised by heat-shock (Dickinson et al., 2015) to produce JDW59; the knock-in sequence was re-confirmed by PCR amplification and sequencing, using the oligos flanking the homology arms. JDW58 was crossed to CA1200 (*eft-3>TIR1::mRuby*) to generate JDW70. The SEC was then excised (Dickinson et al., 2015) to produce JDW71.

pDD121, pDD363, pDD372, and pDD379 (Dickinson et al., 2018) were gifts from Bob Goldstein (Addgene plasmid numbers are 91833, 91829, 91824, and 91834 respectively). pJW1347 and pJW1759 will be deposited into Addgene's repository and are also available upon request. pJW1347 and pJW1759 were generated by TOPO blunt cloning of PCR products. pJW1779 was generated by Gateway cloning into pDONR221 (Invitrogen). Oligo sequences used to generate these plasmids, the sgRNA, the 3' homology arm, and for genotyping are in the **Key Resources Table**.

C. elegans strains and culture conditions

Animals were maintained using standard culture conditions at 25°C (Brenner, 1974). Animals were synchronized through alkaline hypochlorite treatment of gravid adults to isolate eggs (Porta-de-la-Riva et al., 2012). In the main text and figure legends, we designate linkage to a promoter using a greater than symbol (>) and fusion to a protein using a double colon (::). The following alleles and transgenes were used in this manuscript for experimental purposes: LG II: *ieSi57[eft-3>TIR1::mRuby];* LG IV:

ieSi58[eft-3>AID::GFP]; LG X: *wrd10[nhr-25::GFP::AID]*. A complete list of strains used in this manuscript can be found in the **Key Resources Table**.

Auxin experiments

For all post-embryonic auxin experiments, synchronized L1 larval stage animals were first transferred to standard OP50-seeded NGM plates and then transferred at the P6.p 2-cell stage (mid L3 stage) to OP50-seeded NGM agar plates containing IAA or NAA, or M9 buffer containing NAA. The natural auxin IAA was purchased in powder form from Alfa Aesar (A10556). The synthetic auxin NAA was purchased in powder or liquid form from Sigma-Aldrich (317918 and N1641, respectively). Auxins used in this manuscript are also listed in the **Key Resources Table**.

For auxin experiments on plates, a 250 mM stock solution in 95% ethanol was prepared using powder auxin and stored at -20°C. Auxin was diluted into NGM agar, cooled to approximately 50°C, at the time of pouring plates. Fresh OP50 was used to seed plates. For control experiments, 0.25% ethanol was used as described previously (Zhang et al., 2015). Prior to each auxin experiment in M9 buffer, a fresh 1 mM or 4 mM solution in M9 buffer was prepared using liquid NAA. M9 buffer alone was used as a control. A detailed liquid NAA-based degradation protocol can be found in **Supplementary Material 1**. For auxin experiments in the microfluidic platform, a 4 mM solution in M9 buffer containing *E. coli* strain NA22 was prepared using liquid NAA and stored at 4°C for up to 2 weeks. M9 buffer containing NA22 was used as a control. See **Supplementary Material 2** for a detailed protocol describing the preparation of media for the microfluidic device.

RNAi experiments

RNAi targeting *cul-1* was constructed by cloning 997 bp of synthetic DNA based on its cDNA sequence available on WormBase (wormbase.org) into the highly efficient T444T RNAi vector (Sturm et al., 2018). The synthetic DNA was generated by Integrated DNA Technologies (IDT) as a gBlock gene fragment and cloned into BglII/SalI restriction digested T444T vector using the NEBuilder HiFi DNA Assembly Master Mix (E2621). Oligonucleotides used are listed in the **Key Resources Table**.

Scoring defects in anchor cell (AC) specification

Synchronized L1 stage *nhr-25::GFP::AID; eft-3>TIR1::mRuby* animals were plated onto NGM agar plates containing either control or 4 mM NAA and grown for 24 hours at 25°C until the early L3 stage (P6.p 1-cell stage), after the normal time of AC specification. Animals were mounted on 5% noble agar pads and images were acquired as specified below to score for the presence or absence of an AC, visualized by characteristic morphology using DIC optics. Remaining animals remained on NAA plates and scored for plate level adult phenotypes approximately 24 hours later.

Scoring vulva precursor cell (VPC) arrest

Synchronized L1 stage *nhr-25::GFP::AID; eft-3>TIR1::mRuby* animals were plated onto OP50 NGM agar plates and allowed to grow until the P6.p 1-cell stage. Animals were then washed off plates with M9 and transferred onto NGM agar plates containing either control or 4 mM NAA and grown at 25°C until the mid-L3 stage, after the normal time of P6.p cell division. Animals were mounted on 5% noble agar pads containing 10mM sodium azide and secured with a coverslip. Images were acquired as specified below to score for P6.p divisions using DIC optics. Remaining animals were scored for plate level adult phenotypes approximately 24 hours later as described above.

Image acquisition

Images were acquired using a Hamamatsu Orca EMCCD camera and a Borealis-modified Yokagawa CSU-10 spinning disk confocal microscope with a Plan-APOCHROMAT x 100/1.4 oil DIC objective controlled by MetaMorph software (version: 7.8.12.0). Animals were anesthetized on 5% agarose pads containing 10 mM sodium azide and secured with a coverslip. Imaging on the microfluidic device was performed on a Zeiss AXIO Observer.Z7 inverted microscope using the 40X glycerol immersion objective and DIC and GFP filters controlled by ZEN software (version 2.5). Images were captured using a Hamamatsu C11440 digital camera. For scoring plate level phenotypes, images were acquired using a Moticam CMOS (Motic) camera attached to a Zeiss dissecting microscope.

Image processing and analysis

All acquired images were processed using Fiji software (version: 2.0.0-rc-69/1.52p) (Schindelin et al., 2012). To quantify AC- or VPC-specific degradation of AID::GFP, images were captured at the P6.p 2-cell stage and 4-cell stage (mid L3 stage) at time points 0, 30, 60, 90, and 120 minutes in the absence or presence of auxin. Expression of *eft-3>AID::GFP* was quantified by measuring the mean fluorescence intensity (MFI) of ACs and VPCs subtracted by the MFI of a background region in the image to account for camera noise. Cells were outlined using the freehand selection tool in Fiji. Data were normalized by dividing the MFI in treated or untreated animals at time points 30, 60, 90, and 120 minutes by the average MFI in untreated animals at 0 minutes.

For experiments utilizing RNAi, only ACs were measured due to the mosaic penetrance of RNAi in VPCs (Bourdages et al., 2014; Matus et al., 2014). To quantify AC-specific degradation of AID::GFP in animals fed RNAi overnight, images were captured at the P6.p 2-cell stage before auxin treatment and 60 minutes post-treatment. *eft-3>AID::GFP* expression in the AC was quantified as described above. Data were normalized by dividing the MFI in auxin treated animals by the average MFI in untreated animals.

To analyze *nhr-25::GFP::AID* degradation, GFP levels were quantified by measuring the MFI in individual GFP-expressing nuclei in the AC/VU, AC, or VPCs subtracted by the

MFI of a background region in the image to account for background noise. Nuclei were outlined using the threshold tool in Fiji.

Images of L3 larvae were captured in the *C. elegans* larvae-specific microfluidic device by Keil et al. (2017). To quantify AID::GFP degradation, animals were loaded into the microfluidic chamber and fed NA22 bacteria. Images were captured at time points 0, 30, 60, 90, and 120 minutes with or without auxin. Here, *eft-3>AID::GFP* expression was quantified by measuring the MFI in whole animals subtracted by the MFI of a background region in the image to account for background noise. Whole animals were outlined using the freehand selection tool in Fiji. Data were normalized by dividing the MFI in treated or untreated animals at time points 30, 60, 90, and 120 minutes by the average MFI in untreated animals at timepoints 30, 60, 90, and 120 minutes respectively to account for photobleaching from imaging the same animal.

Graphs were made using Prism software (version: 8.1.2). Figures were made using Adobe Photoshop and Illustrator CS. Cartoons were created with either BioRender (biorender.com) or ChemDraw software (version: 18.0).

Statistical analysis

A power analysis was performed using RStudio software (version: 1.1.463) to determine the sample size (*n*) needed per experiment to achieve a power level of 0.80 or greater (Cohen, 1992; Pollard et al., 2019). Statistical significance was determined using either a two-tailed unpaired Student's t-test or Mann Whitney U test. $P < 0.05$ was considered statistically significant. The figure legends specify when error bars represent the SD or IQR. Data were collected from 2-4 independent experiments.

RESULTS AND DISCUSSION

NAA (synthetic auxin) is a viable alternative to IAA (natural auxin)

Given the recent advances in CRISPR/Cas9-genome editing technology (Dickinson and Goldstein, 2016), the auxin-inducible degron (AID) can be easily inserted into a genomic locus of interest (Röth et al., 2019). Though this technology can be applied with ease, there are certain limitations that exist with the use of the natural auxin indole-3-acetic acid (IAA) such as its limited solubility in water, instability, and lack of applicability. Additionally, the ethanol solvent used to dissolve IAA has been shown to cause rapid changes in *C. elegans* gene expression (Zhang et al., 2015). Also, as previous work examined rates of protein degradation of AID-tagged proteins at low magnification and via western blot analysis using whole adult animals (Zhang et al., 2015), we wished to determine the kinetics of protein degradation at single-cell resolution using spinning disk confocal microscopy. We chose to largely examine the L3 stage of post-embryonic development, due to many of the dynamic cellular behaviors occurring over relatively short time scales (within minutes to hours) in this developmental window, including uterine-vulval attachment and vulval morphogenesis (Gupta et al., 2012).

To analyze the kinetics of AID-mediated degradation in the uterine anchor cell (AC) and underlying vulva precursor cells (VPCs) (**Figure 2**), we utilized a previously published strain expressing AID::GFP and TIR1::mRuby under the same ubiquitously expressed *eft-3* promoter (Zhang et al., 2015). The single-cell abundance of AID::GFP was measured over time in mid L3 stage animals exposed to different concentrations of auxin incorporated into standard *C. elegans* solid culture media (**Figure 3A**). In addition to testing the natural auxin IAA, we wanted to test whether it was possible to perform auxin-inducible degradation in the AC and VPCs using the synthetic auxin analog 1-naphthaleneacetic acid (NAA) (**Figure 3B**). In the presence of ≥ 1 mM IAA or NAA, AID::GFP abundance in the AC and VPCs was reduced to approximately 80% of its initial level within 30 minutes (**Figure 3C-D**). Within 60 minutes, AID::GFP was virtually undetectable (**Figure 3C-D**). These results indicate that NAA can serve as a viable substitute to IAA. While the protein degradation kinetics induced by both forms of auxin are nearly identical, NAA is comparably inexpensive and has greater long-term stability than IAA (Dunlap et al., 1986). Though we did not specifically test for auxin-specific toxicity in *C. elegans*, we did not observe any obvious phenotypes with respect to morphology, fecundity, or developmental timing. Furthermore, no toxicity was reported by Zhang et al. (2015) when using IAA. It is worth noting, however, that higher levels of toxicity was recently observed when using IAA over NAA in studies investigating circadian rhythm biology in *Drosophila* (Chen et al., 2018).

The AID system functions through C. elegans CUL-1 to degrade target proteins

Our work and that of others (Zhang et al. 2015) demonstrates that the AID system functions rapidly to degrade target proteins in *C. elegans*. How *Arabidopsis* TIR1 functions through the *C. elegans* proteasomal degradation pathway is unclear. We therefore depleted the SCF complex by RNAi while targeting AID::GFP in the presence of NAA. This experiment was designed to provide insight into the mechanism through which the AID system depletes proteins in *C. elegans*, and as an intersectional proof-of-concept test of combining NAA-based depletion with a RNAi feeding approach. CUL-1, which is known to interact with eight of the Skp1-related proteins in *C. elegans*, including SKR-1, -2, -3, -4, -7, -8, -9 and -10 (Nayak et al., 2002; Yamanaka et al., 2002), is the sole constant in the SCF complex (Kipreos, 2005). As such, we decided to perturb *cul-1* expression. To deplete CUL-1, we generated a new RNAi construct targeting *cul-1* in the upgraded T444T RNAi targeting vector (Sturm et al., 2018). Notably, this vector contains T7 terminator sequences, which prevents non-specific RNA fragments from being synthesized from the vector backbone (Sturm et al., 2018). This vector modification increases the efficiency of mRNA silencing over the original L4440 vector (Medwig-Kinney et al., 2019; Sturm et al., 2018).

We hypothesized that depleting CUL-1 would strongly interfere with the proteasomal machinery, and thus protein turnover. To assess the abundance of AID::GFP in the *C. elegans* AC, we treated animals with either *control(RNAi)* or *cul-1(RNAi)*. Once again, we made use of a strain expressing AID::GFP and TIR1::mRuby from the same *eft-3* driver (Zhang et al. 2015), and we examined animals at the P6.p 2-cell stage (**Figure 4A**). RNAi knockdown of *cul-1* resulted in a modest, but statistically significant increase

in the abundance of AID::GFP in the AC compared to *control(RNAi)* treatment (+19%, *n* = 31 and 33, respectively, *P* < 0.0001) (**Figure 4B**). These results are consistent with findings from a previous study (Munkácsy et al., 2016) which revealed that depletion of *cul-1* by RNAi increased the systemic expression of a transcriptional GFP reporter of β-tubulin, *tbb-6*. In sum, our results further establish CUL-1 as an important mediator of proteasomal degradation and protein homeostasis.

Next, we wanted to determine whether depletion of *cul-1* could inactivate AID-mediated protein degradation. To do this, we fed synchronized L1 stage animals with RNAi targeting *cul-1*. We then treated animals at the P6.p 2-cell stage with 1 mM NAA for 60 minutes and quantified AID::GFP degradation in the AC (**Figure 4A**). For *control(RNAi)*-treated animals, the abundance of AID::GFP in the AC was nearly undetectable within 60 minutes (-94%, *n* = 33) (**Figure 4C**). Remarkably, the abundance of AID::GFP in the AC was reduced by only 29% within 60 minutes for animals treated with *cul-1(RNAi)* (*n* = 31, *P* < 0.0001) (**Figure 4C**). These results suggest that: i) suppression of *cul-1* is sufficient to block TIR1-mediated degradation; ii) TIR1 can function as a substrate recognition component of the *C. elegans* CUL-1-based SCF complex; and iii) it is possible to deplete multiple targets simultaneously using both AID and RNAi technology.

Inhibiting the expression of *cul-1* is a valid approach for reversing AID-mediated degradation in *C. elegans*; we suggest using *cul-1(RNAi)* for this purpose with caution, as CUL-1 has known cell cycle-dependent functions and therefore silencing it may conflate the recovery of AID-tagged proteins with a cell cycle phenotype (Kipreos et al., 1996). As an alternative approach to achieving recovery of AID-tagged proteins, we propose the use of RNAi targeting TIR1 or simply using auxinole, a commercially available inhibitor of TIR1 (Hayashi et al., 2012; Yesbolatova et al., 2019). One caveat to this approach is that auxinole is expensive and thus it may be difficult to obtain stoichiometrically equivalent amounts of auxin and auxinole to truly achieve recovery of one's protein of interest. However, for *C. elegans* researchers requiring tighter temporal control, these may be avenues worth exploring. Presently, recovery from degradation with 1 mM auxin takes up to 24 hours to fully recover expression of the target protein (Zhang et al., 2015). Such protein recovery kinetics are insufficient for studying events in the nematode that occur within minutes to hours such as uterine-vulval attachment, vulval morphogenesis, or many other developmental events occurring post-embryonically.

NAA enables the exploration of developmental phenotypes

As our previous experiments demonstrated that we could effectively deplete a non-functional AID::GFP reporter expressed in the uterine AC and VPCs we next wished to test whether NAA depletion of target proteins could be utilized to study post-embryonic developmental events occurring over a tight temporal window. Thus, we focused on a well-studied system of organogenesis, *C. elegans* uterine-vulval cell specification and morphogenesis (**Figure 2**) (Schindler and Sherwood, 2013). As a proof-of-principle, we chose to deplete the nuclear hormone receptor, *nhr-25,* a homolog of arthropod Ftz-F1

and vertebrate SF-1/NR5A1 and LRH-1/NR5A2, which has been shown to function pleiotropically in a wide array of developmental events, from larval molting (Asahina et al., 2000; Frand et al., 2005; Gissendanner and Sluder, 2000), heterochrony (Hada et al., 2010), and uterine-vulval morphogenesis (Asahina et al., 2006; Chen et al., 2004; Hwang et al., 2007; Hwang and Sternberg, 2004; Ward et al., 2013). It was this pleiotropy that made targeting NHR-25 an attractive target, as RNAi and mutant analyses have shown previously that it is initially required in the AC during the AC/VU decision for proper specification of AC fate (Asahina et al., 2006; Hwang and Sternberg, 2004) and approximately 7 hours later it is required in the underlying VPCs for cell division (Chen et al., 2004; Hwang et al., 2007; Ward et al., 2013).

First, we examined the *nhr-25::GFP::AID* expression pattern, and saw GFP localization to the nuclei of the AC/VU cells during the mid L2 stage, enrichment in the AC following specification, and nuclear localization in the 1˚ and 2˚ VPCs during all stages of vulval division and morphogenesis (**Figure 5A**). We quantified GFP fluorescence over developmental time, and consistent with previous reports based on transgene analyses (Gissendanner and Sluder, 2000; Ward et al., 2013), endogenous NHR-25::GFP::AID AC expression peaks after AC specification in the early L3 at the P6.p 1-cell stage, and is undetectable above background by the P6.p 4-cell stage at the time of AC invasion. Conversely, NHR-25::GFP::AID increases in intensity in the VPCs at the P6.p 4-cell stage peaking during the morphogenetic events occurring following AC invasion (**Figure 5B**). Given this temporally-driven expression pattern and based on previous experimental results from RNAi and mutant analyses (Asahina et al., 2006; Chen et al., 2004; Hwang et al., 2007; Hwang and Sternberg, 2004; Ward et al., 2013), we hypothesized that depleting AID-tagged NHR-25 prior to AC specification should interfere with the AC/VU decision. To test this, we exposed synchronized L1 stage animals expressing *eft-3>TIR1::mRuby* and endogenously tagged NHR-25::GFP::AID to control and 4 mM NAA and examined animals in the early L3 stage, after the normal time of AC specification. Strikingly, all 36 animals examined showed a failure to specify the AC fate, with the presence of either one (10/36) or two (26/36) small AC/VU-like cells in the central gonad as compared to control animals (**Figure 5C**). Next, we repeated the experiment but waited until after AC specification, in the early L3 stage, to expose animals to control or 4 mM NAA. Here, in all animals we detected the presence of an AC situated over P6.p but in 34/36 animals P6.p failed to divide as compared to controls at the mid-L3 stage (**Figure 5D**). Quantification of *nhr-25::GFP::AID* in AC/VU cells (**Figure 5E**) and VPCs (**Figure 5F**) demonstrated the 4 mM NAA treatment robustly depleted endogenous protein by 94% in the AC/VU and 83% in the VPCs, respectively. Finally, we waited until treated animals became adults (about 24 hours later) and examined them for plate level phenotypes. In both cases, we saw a 100% Egg-laying defect (Egl) in 4 mM NAA treated animals as compared to control treated plates (**Figure 5G**). Together, these results indicate that the synthetic auxin, NAA, can robustly deplete target endogenous proteins in an easy, high-throughput fashion, during uterine-vulval development, which should be invaluable in dissecting pleiotropic gene function going forward.

NAA can be solubilized in physiological buffer

Though it is possible to perform a simple dilution of the natural auxin IAA in M9 buffer, it must first be dissolved in ethanol prior to dilution. NAA, on the other hand, can be readily dissolved in water, circumventing the need to dissolve it in ethanol, a solvent known to induce changes in gene expression in as little as 15 minutes in *C. elegans* (Kwon et al., 2004). Since NAA can be solubilized in water-based solutions devoid of ethanol, it has a clear advantage over IAA. Similar to the AID-mediated degradation kinetics observed on NGM plates containing auxin (**Figure 3**), the AID::GFP abundance in the AC and VPCs was measured over time in mid L3 stage animals exposed to different concentrations of NAA solubilized in M9 buffer (**Figure 6A-D**). In the presence of ≥ 1 mM liquid NAA, AID::GFP in the AC and VPCs was reduced by 80%, as compared to initial levels, within 30 minutes and nearly undetectable within 60 minutes (**Figure 6B-D**). These results show that NAA can induce auxin-dependent degradation in liquified form in *C. elegans*.

NAA: an option for the C. elegans microfluidics community

The ability to easily solubilize synthetic auxin in water raises the possibility of performing protein degradation experiments paired with microfluidics where the precise timing of auxin treatment can be precisely controlled. Moreover, individual animals can be imaged over long periods at cellular resolution. To test this, we time-lapsed L3 stage animals using a microfluidic device optimized for long-term imaging of *C. elegans* larvae (Keil et al., 2017), assessing depletion of ubiquitously expressed AID::GFP in trapped animals (**Figure 6A**). At the L3 stage, animals were loaded into the microfluidic chamber in M9 and flushed with a mixture of M9, 4 mM NAA, and NA22 *E. coli* as a bacterial food source (Keil et al., 2017). The animals were imaged every 30 minutes for 2 hours. During image acquisition animals were temporarily immobilized by increasing the negative pressure on the compression layer of the device controlled in an automated fashion (Keil et al., 2017). Between timepoints animals were allowed to move and feed freely in 4 mM NAA combined with NA22 in M9. Although degradation kinetics were slower than those observed in NAA solubilized in M9 alone (**Figure 6C-D**) we still observed nearly 80% depletion of whole animal AID::GFP within 1 hour, and approximately 60% reduction of AID::GFP expression within the first 30 minutes of NAA exposure (**Figure 6E-F**). Our results may be under-representing the overall loss of AID::GFP as we did not account for gut autofluorescence in our quantification of fluorescence intensity in whole animals (Teuscher and Ewald, 2018). Thus, our results here demonstrate that AID-tagged proteins can be depleted in a microfluidic platform, which when combined with long-term high-resolution imaging should provide a powerful tool for studying post-embryonic *C. elegans* development at cellular resolution.

Conclusions

The ease of editing the *C. elegans* genome using CRISPR/Cas9-based approaches (Calarco and Friedland, 2015), when paired with heterologous gene manipulation tools, is ushering in a new era in our understanding of cellular and developmental biology. Several new tools require the insertion of small amino acid tags into target loci including

ZF1 tagging (Armenti et al., 2014), sortase A- (Wu et al., 2017), and the auxin-inducible degron (Zhang et al. 2015). Alternatively, any GFP fusion can be targeted via a GFP nanobody tethered to ZIF1 (Wang et al., 2017). These genomic edits are then paired with single transgene expression to allow for targeted spatial and temporal loss-of-function approaches through manipulation of endogenous loci. These techniques have been largely missing from the *C. elegans* genomic toolkit. With an ever-increasing set of these tools being optimized for *C. elegans*, it is clear that different tools will have strengths and weaknesses depending on multiple variables, including subcellular localization of target protein, availability of tissue- and cell-type specific drivers, and inducibility of depletion. Here, we optimize a powerful heterologous system, the auxin-inducible degradation system, demonstrating that a water-soluble synthetic auxin analog, NAA, can function equivalently to natural auxin. The increase in water solubility allows for easier preparation of media and for performing experiments in liquid culture and microfluidics. We demonstrate the strength of the AID system by examining multiple spatial and temporal roles for the Ftz-F1 homolog *nhr-25* during uterine and vulval morphogenesis. It is our hope that the use of the synthetic NAA will allow *C. elegans* researchers to expand the use of the AID system to examine targeted protein depletion phenotypes in their tissues and developmental stages of interest. As the library of tissue-specific TIR1 drivers grows, we envision researchers being able to rapidly deplete proteins of interest in specific tissues and visualize the outcome at single-cell resolution.

ACKNOWLEDGEMENTS

We thank R. Adikes for the suggestion to look into a water-soluble form of auxin and the Citovsky lab for providing the initial aliquot of NAA. We thank Natalia Stec for help with the microfluidic device. We thank R. Adikes, J. Smith, N. Palmisano, and T. Medwig-Kinney for insightful discussions while developing the NAA liquid protocol and R. Adikes for helpful advice regarding image acquisition parameters and quantification. We thank R. Adikes, N. Palmisano, A. Kohrman and T. Medwig-Kinney for advice and comments on the manuscript. We appreciate the help of Wan Zhang for preparing media and plates.

This work was funded by the National Institute of Health (NIH) National Institute of General Medical Sciences (NIGMS) [1R01GM121597-01 to D.Q.M.]. D.Q.M. is also a Damon Runyon-Rachleff Innovator supported (in part) by the Damon Runyon Cancer Research Foundation [DRR-47-17]. M.A.M. is supported by NIGMS [2T32GM007518-41]. C.M.H and B.A.K. are supported by NIGMS [R01GM117406]. J.D.W. is supported by the NIGMS [R00GM-107345]. Some strains were provided by the Caenorhabditis Genetics Center, which is funded by the NIH Office of Research Infrastructure Programs [P40 OD010440].

AUTHOR CONTRIBUTIONS

M.A.M. and D.Q.M conceived and designed the experiments. G.A. and J.D.W. designed the constructs. J.M.R. performed the microinjections. G.A. performed the crosses and

characterized strains. M.A.M. and B.A.K. performed the experiments. M.A.M. and D.Q.M. analyzed and quantified the data. M.A.M. and D.Q.M. wrote the manuscript with contributions from the other authors. The authors declare no competing interests.

REFERENCES

Armenti, S.T., Lohmer, L.L., Sherwood, D.R., Nance, J., 2014. Repurposing an endogenous degradation system for rapid and targeted depletion of *C. elegans* proteins. Development 141, 4640–4647. https://doi.org/10.1242/dev.115048

Asahina, M., Ishihara, T., Jindra, M., Kohara, Y., Katsura, I., Hirose, S., 2000. The conserved nuclear receptor Ftz-F1 is required for embryogenesis, moulting and reproduction in *Caenorhabditis elegans*. Genes to Cells 5, 711–723.

Asahina, M., Valenta, T., Silhankova, M., Korinek, V., Jindra, M., 2006. Crosstalk between a Nuclear Receptor and β-Catenin Signaling Decides Cell Fates in the C. elegans Somatic Gonad. Dev. Cell 11, 203–211. https://doi.org/10.1016/j.devcel.2006.06.003

Bourdages, K.G., Lacroix, B., Dorn, J.F., Descovich, C.P., Maddox, A.S., 2014. Quantitative analysis of cytokinesis In Situduring *C. elegans* postembryonic development. PLoS One 9. https://doi.org/10.1371/journal.pone.0110689

Brenner, S., 1974. The genetics of *Caenorabditis elegans*. Genetics 77, 71–94. https://doi.org/10.1016/S0047-2484(78)80101-8

Calarco, J.A., Friedland, A.E., 2015. Creating Genome Modifications in *C. elegans* Using the CRISPR/Cas9 System, Methods in Molecular Biology. https://doi.org/10.1007/978-1-4939-2842-2_6

Chen, W., Werdann, M., Zhang, Y., 2018. The auxin-inducible degradation system enables conditional PERIOD protein depletion in the nervous system of *Drosophila melanogaster*. FEBS J. 285, 4378–4393. https://doi.org/10.1111/febs.14677

Chen, Z., Eastburn, D.J., Han, M., 2004. The *Caenorhabditis elegans* Nuclear Receptor Gene *nhr-25* Regulates Epidermal Cell Development. Mol. Cell. Biol. 24, 7345–7358. https://doi.org/10.1128/mcb.24.17.7345-7358.2004

Cohen, J., 1992. A Power Primer. Psychol. Bull. 112, 155–159.

Daniel, K., Icha, J., Horenburg, C., Müller, D., Norden, C., Mansfeld, J., 2018. Conditional control of fluorescent protein degradation by an auxin-dependent nanobody. Nat. Commun. 9. https://doi.org/10.1038/s41467-018-05855-5

Dickinson, D.J., Goldstein, B., 2016. CRISPR-based methods for *Caenorhabditis elegans* genome engineering. Genetics 202, 885–901. https://doi.org/10.1534/genetics.115.182162

Dickinson, D.J., Pani, A.M., Heppert, J.K., Higgins, C.D., Goldstein, B., 2015. Streamlined Genome Engineering with a Self-Excising Drug Selection Cassette 200, 1035–1049. https://doi.org/10.1534/genetics.115.178335

Dickinson, D.J., Slabodnick, M.M., Chen, A.H., Goldstein, B., 2018. SapTrap assembly of repair templates for Cas9-triggered homologous recombination with a self-excising cassette. microPublication Biol. https://doi.org/10.17912/W2KT0N

Dickinson, D.J., Ward, J.D., Reiner, D.J., Goldstein, B., 2013. Engineering the *Caenorhabditis elegans* genome using Cas9-triggered homologous recombination. Nat. Methods 10, 1028–1034. https://doi.org/10.1038/nmeth.2641

Dunlap, J.R., Kresovich, S., McGee, R.E., 1986. The Effect of Salt Concentration on Auxin Stability in Culture Media. Plant Physiol. 81, 934–936. https://doi.org/10.1104/pp.81.3.934

Frand, A.R., Russel, S., Ruvkun, G., 2005. Functional genomic analysis of *C. elegans*

molting. PLoS Biol. 3. https://doi.org/10.1371/journal.pbio.0030312

Frøkjær-Jensen, C., Davis, M.W., Ailion, M., Jorgensen, E.M., 2012. Improved Mos1-mediated transgenesis in *C. elegans*. Nat. Methods 9, 117–118. https://doi.org/10.1038/nmeth.1865

Gissendanner, C.R., Sluder, A.E., 2000. *nhr-25*, the *Caenorhabditis elegans* ortholog of ftz-f1, is required for epidermal and somatic gonad development. Dev. Biol. 221, 259–272. https://doi.org/10.1006/dbio.2000.9679

Gupta, B.P., Hanna-Rose, W., Sternberg, P.W., 2012. Morphogenesis of the vulva and the vulval-uterine connection. WormBook 1–20. https://doi.org/10.1895/wormbook.1.152.1

Hada, K., Asahina, M., Hasegawa, H., Kanaho, Y., Slack, F.J., Niwa, R., 2010. The nuclear receptor gene nhr-25 plays multiple roles in the *Caenorhabditis elegans* heterochronic gene network to control the larva-to-adult transition. Dev. Biol. 344, 1100–1109. https://doi.org/10.1016/j.ydbio.2010.05.508

Hayashi, K.I., Neve, J., Hirose, M., Kuboki, A., Shimada, Y., Kepinski, S., Nozaki, H., 2012. Rational design of an auxin antagonist of the SCF TIR1 auxin receptor complex. ACS Chem. Biol. 7, 590–598. https://doi.org/10.1021/cb200404c

Holland, A.J., Fachinetti, D., Han, J.S., Cleveland, D.W., 2012. Inducible, reversible system for the rapid and complete degradation of proteins in mammalian cells. Proc. Natl. Acad. Sci. 109, E3350–E3357. https://doi.org/10.1073/pnas.1216880109

Hubbard, E.J.A., 2014. FLP/FRT and Cre/lox recombination technology in *C. elegans*. Methods 68, 417–424. https://doi.org/10.1016/j.ymeth.2014.05.007

Hwang, B.J., Meruelo, A.D., Sternberg, P.W., 2007. *C. elegans* EVI1 proto-oncogene, EGL-43, is necessary for Notch-mediated cell fate specification and regulates cell invasion. Development 134, 669–679. https://doi.org/10.1242/dev.02769

Hwang, B.J., Sternberg, P.W., 2004. A cell-specific enhancer that specifies lin-3 expression in the *C. elegans* anchor cell for vulval development. Development 131, 143–151. https://doi.org/10.1242/dev.00924

Keil, W., Kutscher, L.M., Shaham, S., Siggia, E.D., 2017. Long-Term High-Resolution Imaging of Developing *C. elegans* Larvae with Microfluidics. Dev. Cell 40, 202–214. https://doi.org/10.1016/j.devcel.2016.11.022

Kipreos, E., 2005. Ubiquitin-mediated pathways in *C. elegans*. WormBook 1–24. https://doi.org/10.1895/wormbook.1.36.1

Kipreos, E.T., Lander, L.E., Wing, J.P., He, W.W., Hedgecock, E.M., 1996. *cul-1* is required for cell cycle exit in *C. elegans* and identifies a novel gene family. Cell 85, 829–839. https://doi.org/10.1016/S0092-8674(00)81267-2

Kwon, J.Y., Hong, M., Choi, M.S., Kang, S., Duke, K., Kim, S., Lee, S., Lee, J., 2004. Ethanol-response genes and their regulation analyzed by a microarray and comparative genomic approach in the nematode *Caenorhabditis elegans*. Genomics 83, 600–614. https://doi.org/10.1016/j.ygeno.2003.10.008

Matus, D.Q., Chang, E., Makohon-Moore, S.C., Hagedorn, M.A., Chi, Q., Sherwood, D.R., 2014. Cell division and targeted cell cycle arrest opens and stabilizes basement membrane gaps. Nat. Commun. 5, 1–13. https://doi.org/10.1038/ncomms5184

Medwig-Kinney, T.N., Smith, J.J., Palmisano, N.J., Zhang, W., Matus, D.Q., 2019. A

developmental gene regulatory network for invasive differentiation of the *C. elegans* anchor cell. bioRxiv. https://doi.org/http://dx.doi.org/10.1101/691337

Munkácsy, E., Khan, M.H., Lane, R.K., Borror, M.B., Park, J.H., Bokov, A.F., Fisher, A.L., Link, C.D., Rea, S.L., 2016. DLK-1, SEK-3 and PMK-3 Are Required for the Life Extension Induced by Mitochondrial Bioenergetic Disruption in *C. elegans*. PLoS Genet. 12, 1–37. https://doi.org/10.1371/journal.pgen.1006133

Nayak, S., Santiago, F.E., Jin, H., Lin, D., Schedl, T., Kipreos, E.T., 2002. The *Caenorhabditis elegans* Skp1-related gene family: Diverse functions in cell proliferation, morphogenesis, and meiosis. Curr. Biol. 12, 277–287. https://doi.org/10.1016/S0960-9822(02)00682-6

Nishimura, K., Fukagawa, T., Takisawa, H., Kakimoto, T., Kanemaki, M., 2009. An auxin-based degron system for the rapid depletion of proteins in nonplant cells. Nat. Methods 6, 917–922. https://doi.org/10.1038/nmeth.1401

Pollard, D.A., Pollard, T.D., Pollard, K.S., 2019. Empowering statistical methods for cellular and molecular biologists. Mol. Biol. Cell 30, 1359–1368. https://doi.org/10.1091/mbc.E15-02-0076

Porta-de-la-Riva, M., Fontrodona, L., Villanueva, A., Cerón, J., 2012. Basic *Caenorhabditis elegans* Methods: Synchronization and Observation. J. Vis. Exp. 1–9. https://doi.org/10.3791/4019

Qadota, H., Inoue, M., Hikita, T., Köppen, M., Hardin, J.D., Amano, M., Moerman, D.G., Kaibuchi, K., 2007. Establishment of a tissue-specific RNAi system in *C. elegans*. Gene 400, 166–173. https://doi.org/10.1016/j.gene.2007.06.020

Röth, S., Fulcher, L.J., Sapkota, G.P., 2019. Advances in targeted degradation of endogenous proteins. Cell. Mol. Life Sci. https://doi.org/10.1007/s00018-019-03112-6

Schindelin, J., Arganda-Carreras, I., Frise, E., Kaynig, V., Longair, M., Pietzsch, T., Preibisch, S., Rueden, C., Saalfeld, S., Schmid, B., Tinevez, J.-Y., White, D.J., Hartenstein, V., Eliceiri, K., Tomancak, P., Cardona, A., 2012. Fiji: an open-source platform for biological-image analysis. Nat. Methods 9, 676–82. https://doi.org/10.1038/nmeth.2019

Schindler, A.J., Sherwood, D.R., 2013. Morphogenesis of the *Caenorhabditis elegans* vulva. Wiley Interdiscip. Rev. Dev. Biol. 2, 75–95. https://doi.org/10.1002/wdev.87

Schwartz, M.L., Jorgensen, E.M., 2016. SapTrap, a toolkit for high-throughput CRISPR/Cas9 gene modification in *Caenorhabditis elegans*. Genetics 202, 1277–1288. https://doi.org/10.1534/genetics.115.184275

Shen, Z., Zhang, X., Chai, Y., Zhu, Z., Yi, P., Feng, G., Li, W., Ou, G., 2014. Conditional knockouts generated by engineered CRISPR-Cas9 endonuclease reveal the roles of coronin in c.elegans neural development. Dev. Cell 30, 625–636. https://doi.org/10.1016/j.devcel.2014.07.017

Sturm, Á., Saskoi, É., Tibor, K., Weinhardt, N., Vellai, T., 2018. Highly efficient RNAi and Cas9-based auto-cloning systems for *C. elegans* research. Nucleic Acids Res. 46, e105. https://doi.org/10.1093/nar/gky516

Teuscher, A., Ewald, C., 2018. Overcoming Autofluorescence to Assess GFP Expression During Normal Physiology and Aging in *Caenorhabditis elegans*. Bio-Protocol 8. https://doi.org/10.21769/bioprotoc.2940

Trost, M., Blattner, A.C., Lehner, C.F., 2016. Regulated protein depletion by the auxin-

inducible degradation system in *Drosophila melanogaster*. Fly (Austin). 10, 35–46. https://doi.org/10.1080/19336934.2016.1168552

Wang, S., Tang, N.H., Lara-Gonzalez, P., Zhao, Z., Cheerambathur, D.K., Prevo, B., Chisholm, A.D., Desai, A., Oegema, K., 2017. A toolkit for GFP-mediated tissue-specific protein degradation in *C. elegans* . Development 144, 2694–2701. https://doi.org/10.1242/dev.150094

Ward, J.D., Bojanala, N., Bernal, T., Ashrafi, K., Asahina, M., Yamamoto, K.R., 2013. Sumoylated NHR-25/NR5A Regulates Cell Fate during *C. elegans* Vulval Development. PLoS Genet. 9. https://doi.org/10.1371/journal.pgen.1003992

Wu, Q., Ploegh, H.L., Truttmann, M.C., 2017. Hepta-Mutant Staphylococcus aureus Sortase A (SrtA7m) as a Tool for in Vivo Protein Labeling in *Caenorhabditis elegans*. ACS Chem. Biol. 12, 664–673. https://doi.org/10.1021/acschembio.6b00998

Yamanaka, A., Yada, M., Imaki, H., Koga, M., Ohshima, Y., Nakayama, K.I., 2002. Multiple Skp1-related proteins in *Caenorhabditis elegans*: Diverse patterns of interaction with Cullins and F-box proteins. Curr. Biol. 12, 267–275. https://doi.org/10.1016/S0960-9822(02)00657-7

Yesbolatova, A., Natsume, T., Hayashi, K. ichiro, Kanemaki, M.T., 2019. Generation of conditional auxin-inducible degron (AID) cells and tight control of degron-fused proteins using the degradation inhibitor auxinole. Methods 0–1. https://doi.org/10.1016/j.ymeth.2019.04.010

Zhang, L., Ward, J.D., Cheng, Z., Dernburg, A.F., 2015. The auxin-inducible degradation (AID) system enables versatile conditional protein depletion in *C. elegans*. Development 142, 4374–4384. https://doi.org/10.1242/dev.129635

Martinez, et al. (2019)

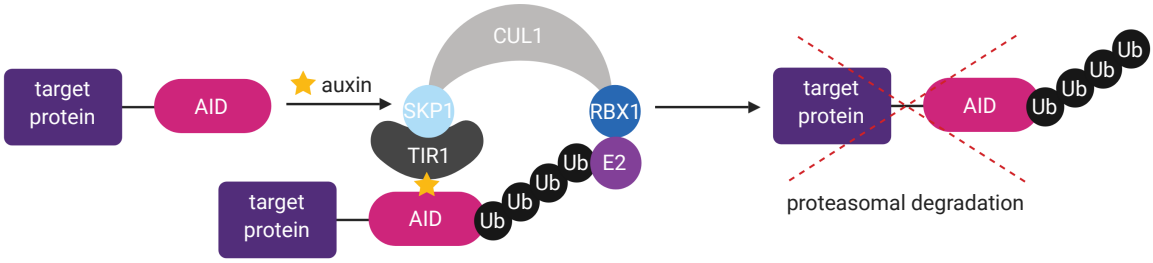

Figure 1. Overview of the auxin-inducible degradation system. In this system, a target protein is fused to an auxin-inducible degron (AID). Heterologous expression of *Arabidopsis* TIR1 mediates robust auxin-dependent proteasomal degradation of AID-tagged proteins through the SKP1-CUL1-F-box (SCF) E3 ubiquitin ligase complex.

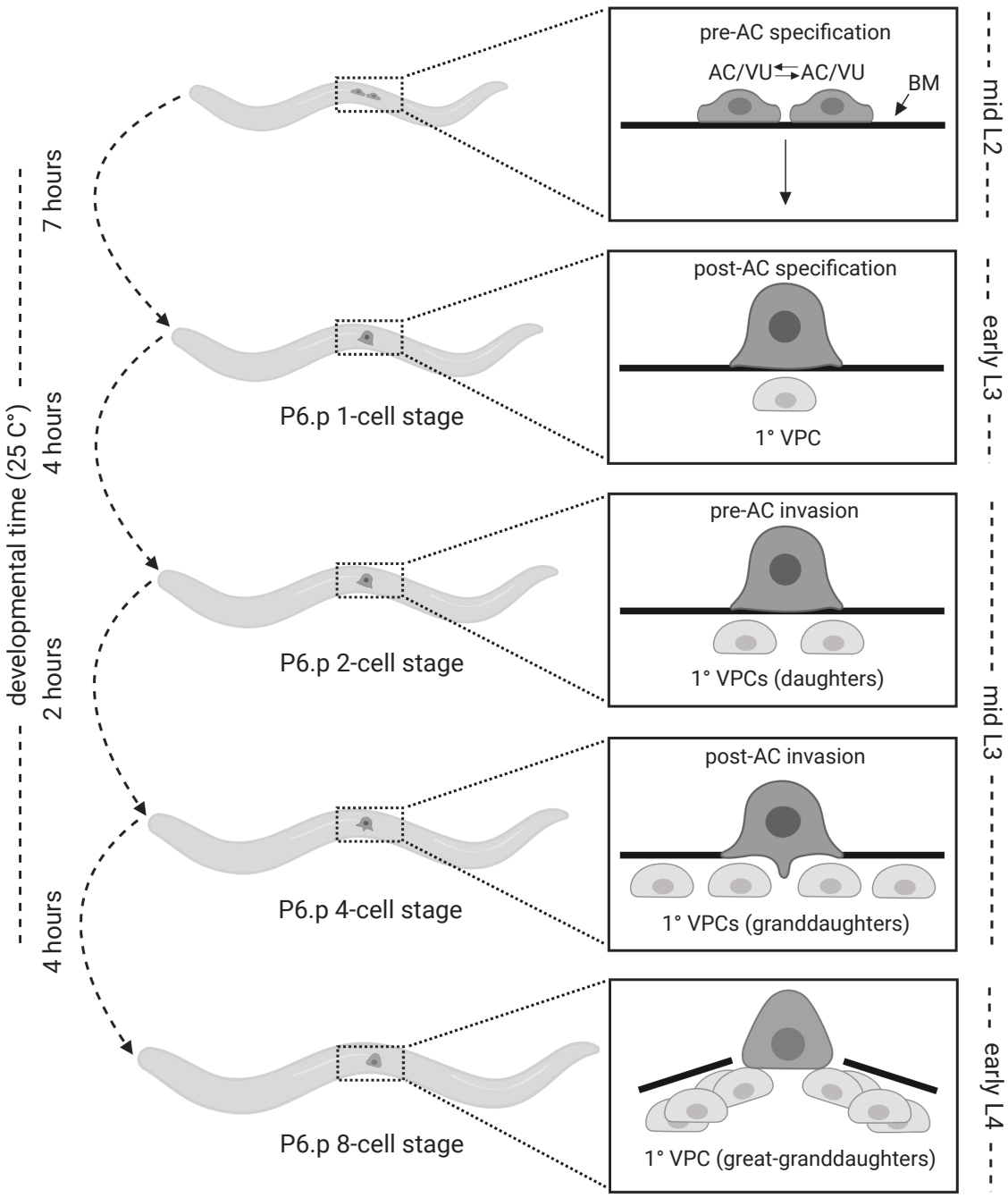

Figure 2. Schematic of uterine-vulval morphogenesis during *C. elegans* larval development. In *C. elegans*, the specification and morphogenesis of uterine-vulval attachment occurs from the mid-L2 through the early L4 stage (Schindler and Sherwood, 2013). The AC is specified in a stochastic reciprocal Notch-Delta signaling event in the mid L2 stage (top panel). Following AC specification, the AC specifies the 1˚ fate of the underlying vulval precursor cell, P6.p in the early L3 (second panel), which then divides three times to ultimately give rise to eight of the 22 cells of the adult vulva (bottom three panels).

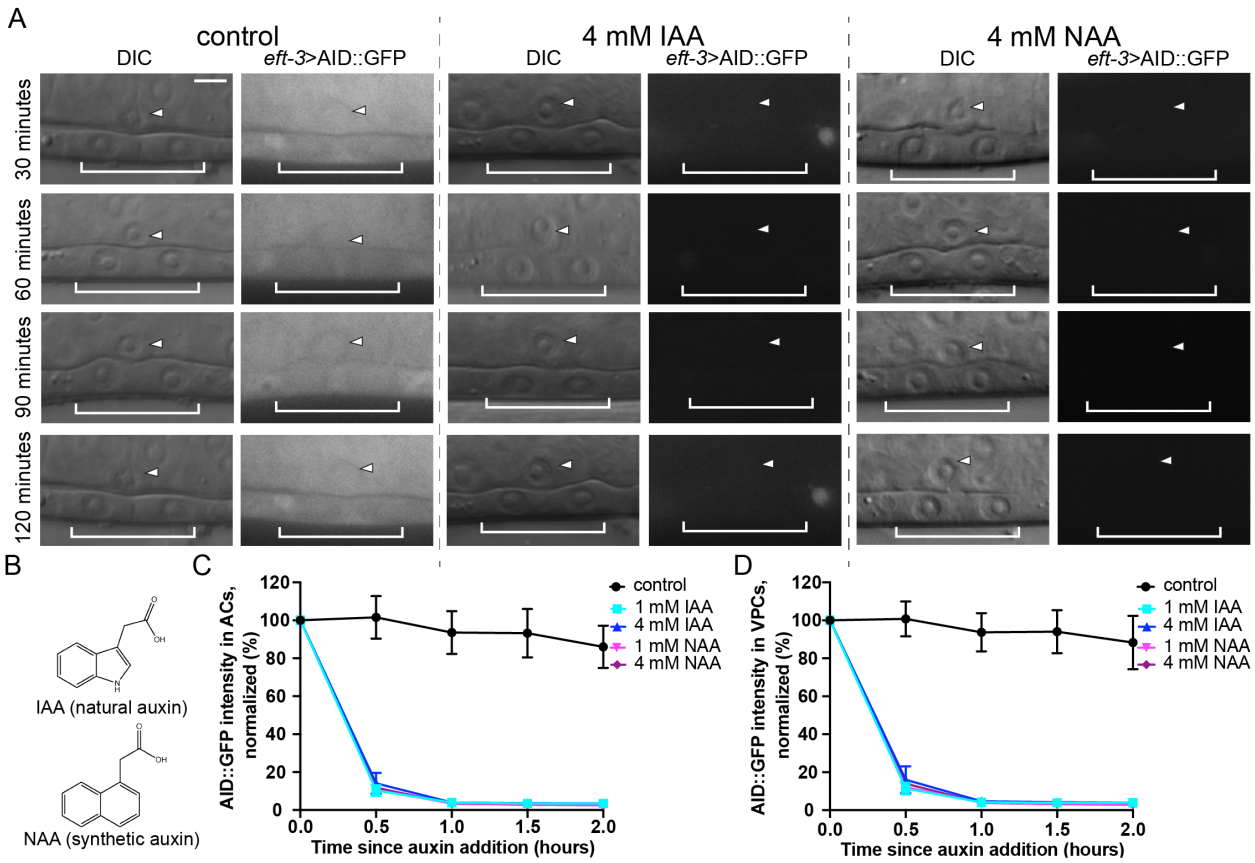

Figure 3. Comparison of IAA- and NAA-mediated degradation in the *C. elegans* AC and VPCs. (A) DIC and corresponding GFP images of ACs (arrowheads) and underlying 1˚ fated VPCs (brackets) from mid L3 stage animals at the P6.p 2-cell stage. Animals expressing AID::GFP and TIR1::mRuby under the same *eft-3* promoter were treated with natural auxin indole-3-acetic acid (IAA) and synthetic auxin 1-naphthaleneacetic acid (NAA) in NGM agar containing OP50. (B) Chemical structure of IAA and NAA. (C, D) Rates of degradation determined by quantifying AID::GFP in (C) ACs and (D) VPCs following auxin treatment. Data presented as the mean±SD ($n \geq 30$ animals examined for each time point).

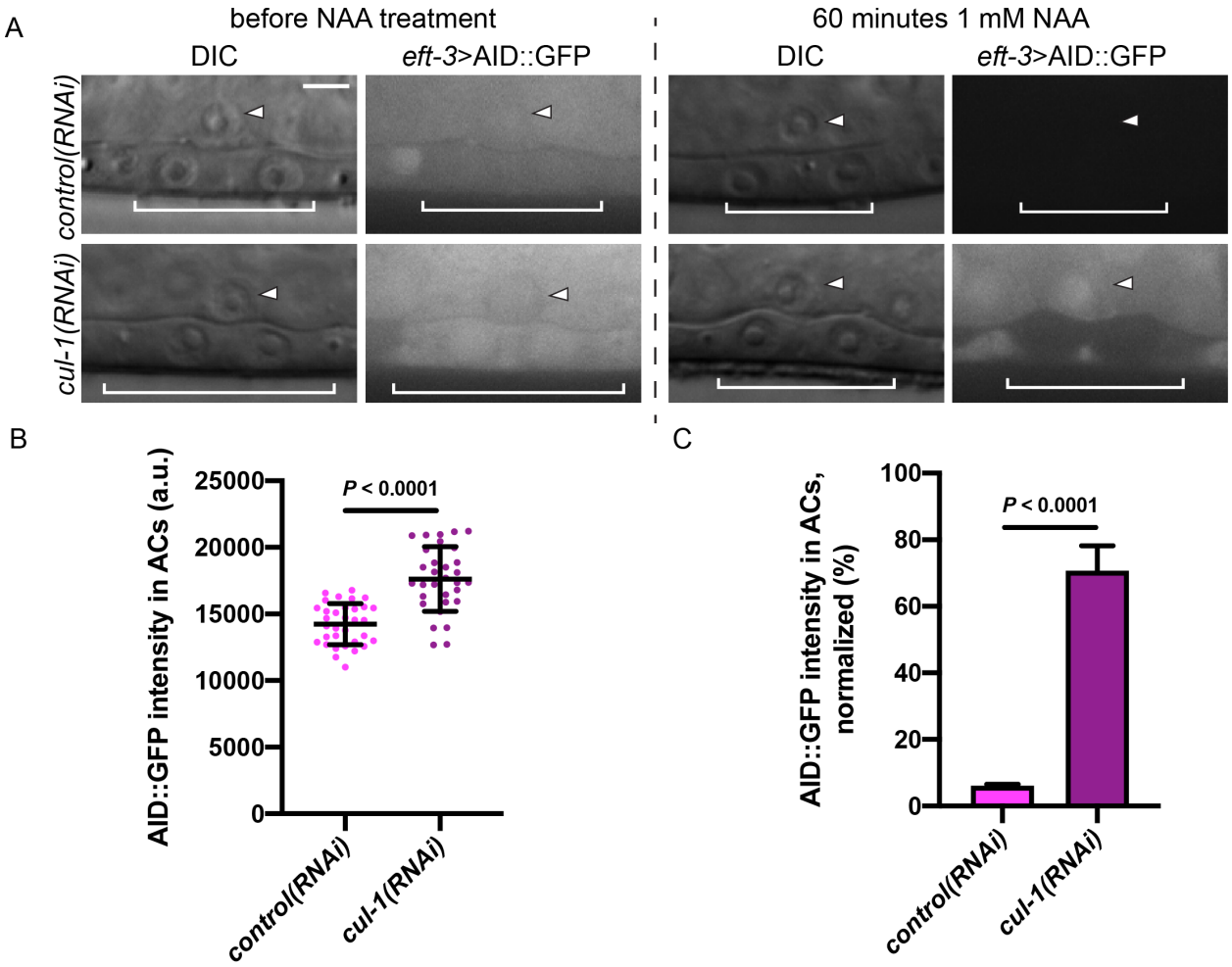

Figure 4. Suppression of *cul-1* expression inhibits TIR1-dependent degradation in the *C. elegans* AC. (A) DIC and corresponding GFP images of ACs (arrowheads) and underlying VPCs (brackets) from mid L3 stage animals at the P6.p 2-cell stage. Animals expressing AID::GFP and TIR1::mRuby under the same *eft-3* promoter were treated with *cul-1(RNAi).* (B) Quantification of AID::GFP in ACs following *cul-1(RNAi)* treatment. Data presented as the mean+SD ($n \geq 30$ animals examined for each, and $P < 0.0001$ by a Student's t-test). (C) Quantification of AID::GFP in ACs following treatment with NAA. Data presented as the median+IQR ($n \geq 30$ animals examined for each, and $P < 0.0001$ by a Mann Whitney U test).

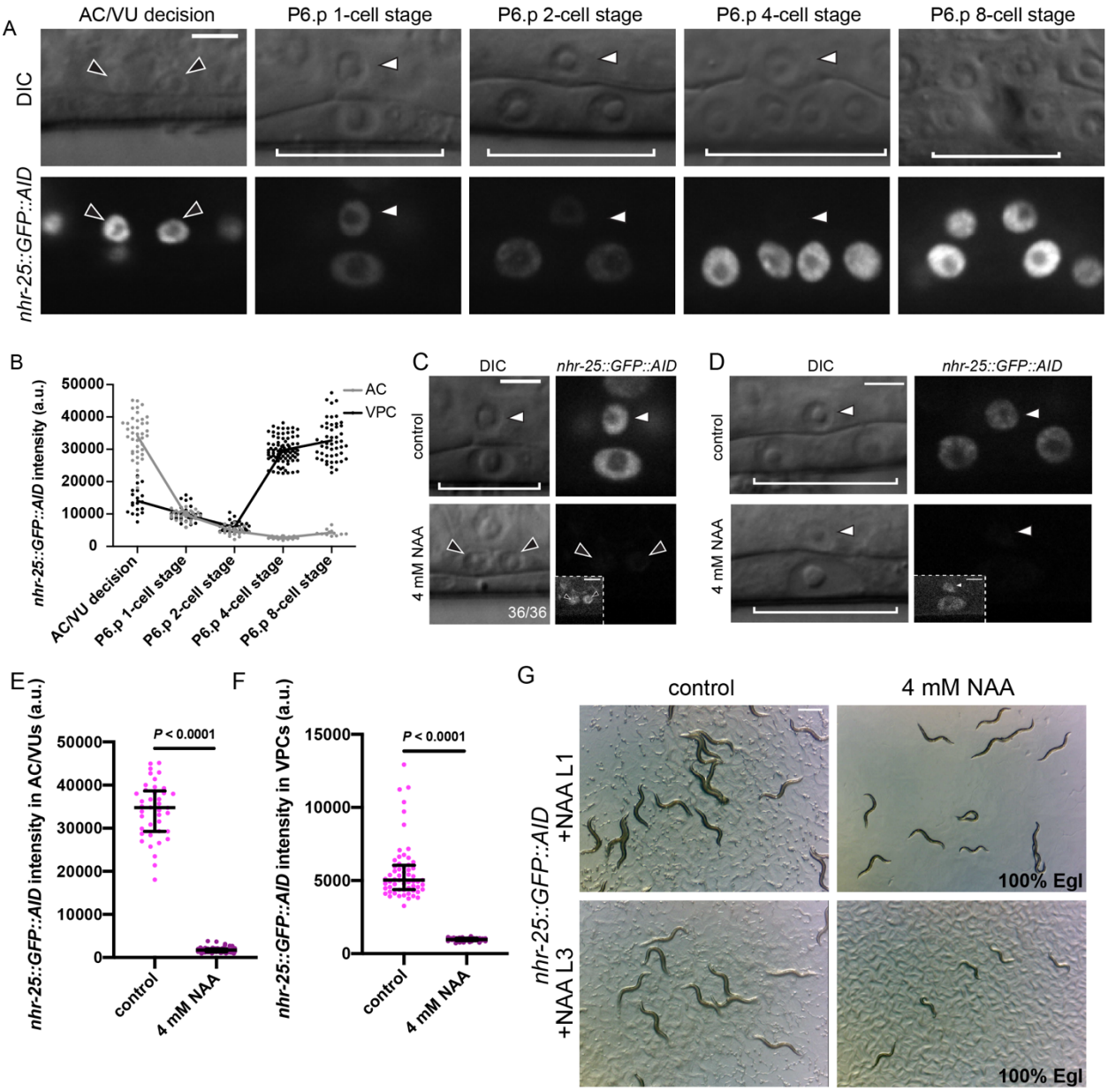

Figure 5. NAA-mediated degradation of NHR-25 causes AC specification and VPC division defects. (A) *nhr-25::GFP::AID* localizes to the nuclei of the AC/VU (black arrowheads), the AC (white arrowheads) and VPCs (brackets). At P6.p 8-cell stage (far right) the AC is not in the same focal plane as the 1˚ VPCs. (B) Quantification of *nhr-25::GFP::AID* over developmental time, from the AC/VU decision to the P6.p 8-cell stage. The curve is connected by the mean at each developmental stage (n = 20, 31, 20, 21, and 12 animals quantified, respectively). (C, D) DIC and corresponding GFP images of ACs (arrowheads) and underlying VPCs (brackets) from (C) early L3 stage animals and (D) mid-L3 stage animals. Animals expressing *nhr-25::AID::GFP* and *eft-3>TIR1::mRuby* were treated with control and 4 mM NAA. (E) Quantification of *nhr-25::GFP::AID* in AC/VUs following NAA treatment. Data presented as the median+IQR ($n \geq 20$ animals examined for each, and $P < 0.0001$ by a Mann Whitney U test). (F) Quantification of *nhr-25::GFP::AID* in VPCs following NAA treatment. Data presented as

the median+IQR ($n \geq 30$ animals examined for each, and $P < 0.0001$ by a Mann Whitney U test). (G) Representative images of adult plate level phenotypes following control and 4 mM NAA treatments added at the L1 (top) and L3 stage (bottom) ($n \geq 130$ animals examined for L1 treatment and $n \geq 30$ animals examined for L3 treatment). Scale bar in (G), 500 μm.

Martinez, et al. (2019)

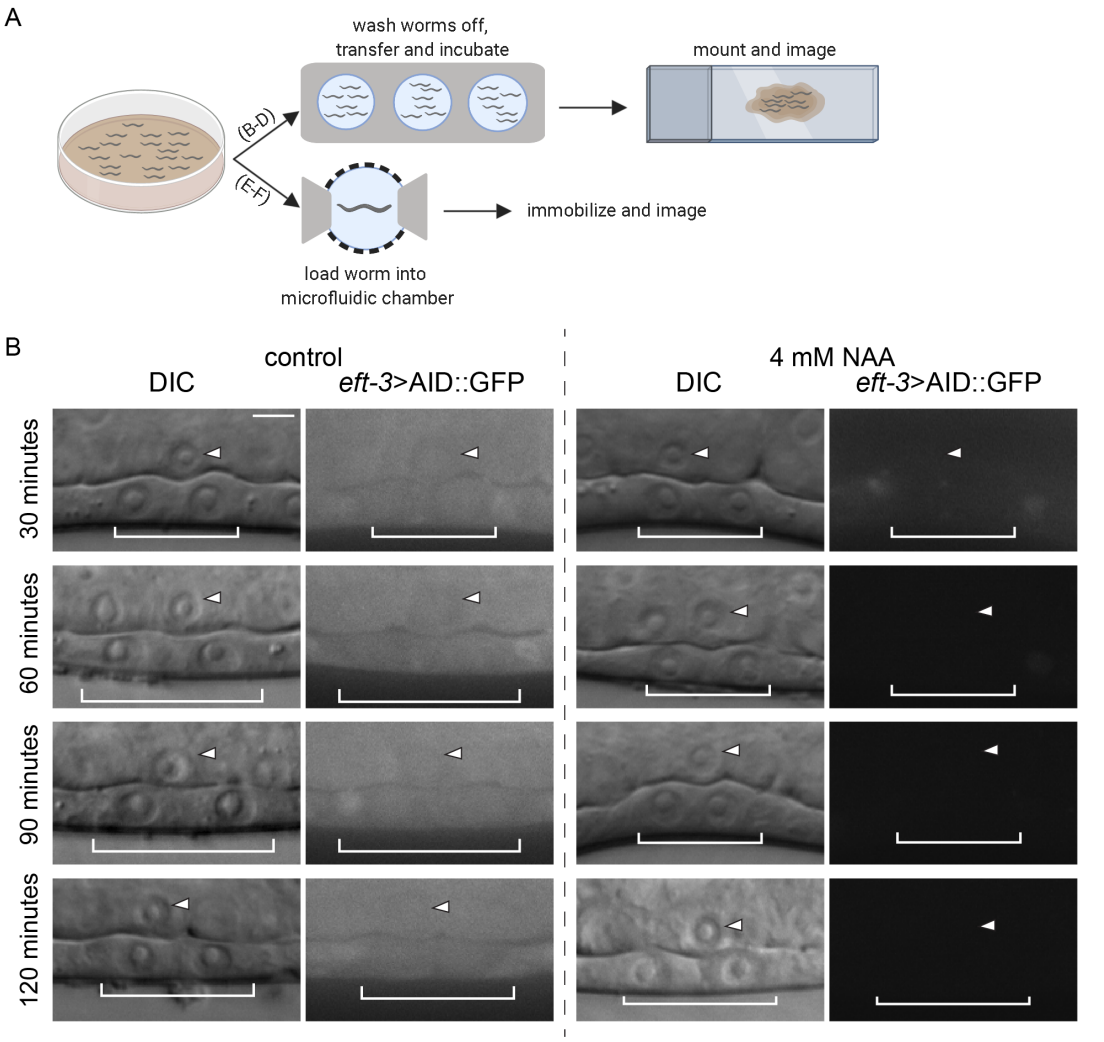

Figure 6. Solubility of NAA in physiological buffer enhances its utility. (A) Schematic representation of the liquid NAA-based degradation protocol for use in high-resolution microscopy or microfluidics-based approaches. (B) DIC and corresponding GFP images of ACs (arrowheads) and underlying VPCs (brackets) from mid L3 stage animals at the P6.p 2-cell stage. Animals expressing AID::GFP and TIR1::mRuby under the same *eft-3* promoter were treated with NAA in M9. (C, D) Rates of degradation were determined by quantifying AID::GFP in (C) ACs and (D) VPCs following auxin treatment. Data presented as the mean±SD ($n \geq 30$ animals examined for each time point). (E) Images of AID::GFP expression from mid L3 stage animals in control conditions (M9 buffer containing NA22 only) or conditions where a 4 mM NAA solution in M9 buffer containing NA22 was perfused through the microfluidic chamber for the time indicated (Keil et al. 2017). (F) Rates of degradation were determined by quantifying AID::GFP in whole animals following auxin treatment. Data presented as the mean±SD ($n \geq 4$ animals examined for each time point).